Composite Materials

DOI: 10.1002/anie.201207825

Size-Dependent Structural Distortions in One-Dimensional Nanostructures**

*Michael D. Anderson, Colby L. Heideman, Qiyin Lin, Mary Smeller, Robert Kokenyesi, Andrew A. Herzing, Ian M. Anderson, Douglas A. Keszler, Paul Zschack, and David C. Johnson**

Nanoscale materials have been intensely studied since the discovery that the optical properties of semiconductor nanoparticles are size dependent.[1–3] This and subsequent research has demonstrated that a given physical property of a particle exhibits a size dependence when the size becomes comparable to its characteristic length scale. Examples of relevant length scales include the de Broglie wavelength and/or the mean free path of electrons, phonons, and elementary excitations, all of which typically range from one to a few hundred nanometers. The ability to tune a wide variety of properties by controlling the particle size has spurred the development of novel chemistries for preparing nanostructured elements and compounds with goals of precisely controlling size, shape, and ligand shell.[4–8]

As the size of a nanocrystal decreases, the ratio of bulk to surface atoms decreases. This progression increases the relative contribution of the surface free-energy relative to the volume free-energy of the bulk structure, such that distortions from bulk equilibrium structures might be expected as the nanoparticle size decreases. Unfortunately, while researchers have demonstrated the ability to prepare ordered lattices of nanoparticles,[9–14] the isolation of lattices of nanoparticles with long-range atomic periodicity is rare.[11,13,15] Hence detailed atomic structures and, in turn, the size-structure-property relationships of most nanoparticle systems cannot readily be determined.[15–17]

Recently we reported that the intergrown compounds $[(MSe)_{1+y}]_m(TSe_2)_n$, with M = {Pb, Bi, Ce} and T = {W, Nb, Ta} self-assemble from designed precursors.[18,19] The values of m and n represent, respectively, the number of MSe and TSe_2 structural units of the unit cell of the superstructure and y describes the misfit between these structural units. As reported herein, the long-range structural order along the modulation direction permits us to determine the atomic structure of these precisely defined one-dimensional (1D) nanolaminate structures as a function of m and n using a combination of scanning transmission electron microscopy (STEM) high-angle annular dark-field (HAADF) imaging and X-ray diffraction (XRD) with Rietveld refinement.

STEM-HAADF images of the first five $[(PbSe)_{1.00}]_m$-$(MoSe_2)_n$ compounds in the family where $m = n$ are shown in Figure 1 along with aggregate intensity plots used to quantify the PbSe intra- and inter-pair distances. All have a regular periodic structure along the modulated axis with well-defined layers of PbSe and $MoSe_2$. The STEM images show ordered domains of PbSe with characteristic dimensions of a single structural unit along the layering direction and tens of nanometers perpendicular to the layering direction, with random in-plane rotational variants both within a layer and between layers. The orientations of the $MoSe_2$ domains are more difficult to discern from the STEM images, but rotational variants have been observed between individual $MoSe_2$ structural units. The STEM-HAADF images reveal a distortion of the PbSe layers, with the atomic planes grouped into pairs rather than being evenly spaced as expected for the equilibrium (bulk) rock salt structure. The distortion is most evident in the structural variant $(m, n) = (2, 2)$ and decreases in magnitude until it can no longer be observed for (5, 5).

[*] Prof. D. C. Johnson
Department of Chemistry, University of Oregon
Eugene, OR, 97403 (USA)
E-mail: davej@uoregon.edu
Homepage: http://pages.uoregon.edu/grnchem/davejohnson.html
Dr. M. D. Anderson, Dr. M. Smeller
Department of Chemistry, University of Oregon, Eugene (USA)
Prof. C. L. Heideman
Department of Chemistry, Eastern Oregon University
LaGrande (USA)
Dr. Q. Lin
Institute for Telecommunications and Information Technology University
University of California, Irvine (USA)
Dr. R. Kokenyesi, Prof. D. A. Keszler
Department of Chemistry, Oregon State University
Corvallis (USA)
Dr. A. A. Herzing, Dr. I. M. Anderson
Surface and Microanalysis Science Division
National Institute of Standards and Technology
Gaithersburg (USA)
Dr. P. Zschack
Advanced Photon Source, Argonne National Laboratory
Argonne (USA)

[**] The authors acknowledge support from the National Science Foundation through grant number DMR 0907049 and by ONR through grant number N00014-07-1-0358. Coauthors M.D.A. and C.L.H. acknowledge support from DGE (grant number 0549503). Coauthors R.K., D.A.K., and D.C.J. acknowledge support from the National Science Foundation through CCI grant number CHE-1102637. Use of the Advanced Photon Source was supported by the U.S. Department of Energy, Office of Science, Office of Basic Energy Sciences, under contract number DE-AC02-06CH11357.

Supporting information for this article is available on the WWW under http://dx.doi.org/10.1002/anie.201207825.

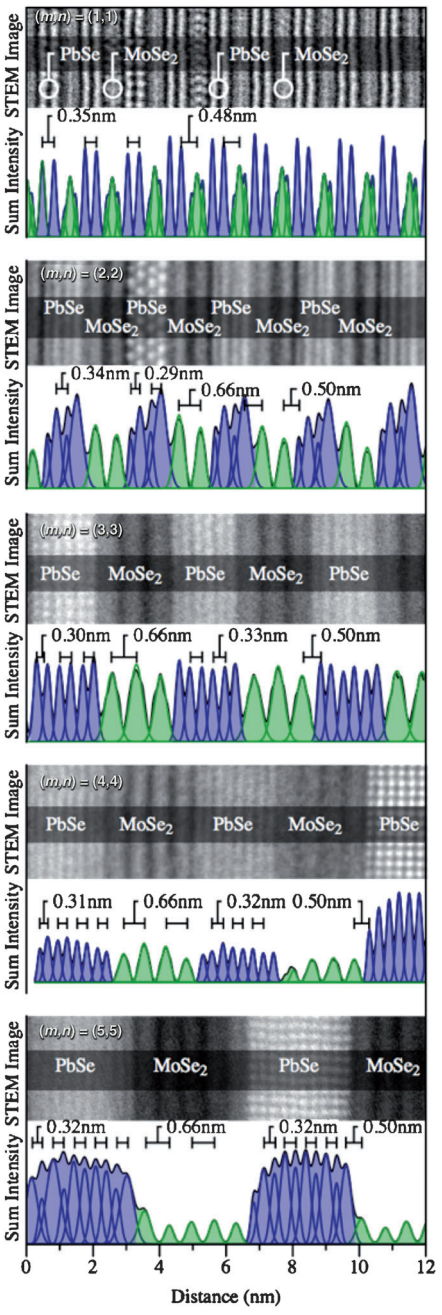

Figure 1. High-resolution STEM-HAADF images of $[(PbSe)_{1.00}]_m(MoSe_2)_n$ compounds in the family $m = n$ with aggregate intensity plots. The rock-salt-structured domains exhibit numerous rotational variants within the (001)-oriented growth plane, with selected grains aligned along the ⟨100⟩- and ⟨110⟩-type zone axes. The distances noted are for the PbSe intra- and inter-pair distances as well as the distances between the last PbSe layer and the central maxima of the $MoSe_2$ region and the distance between consecutive $MoSe_2$ regions.

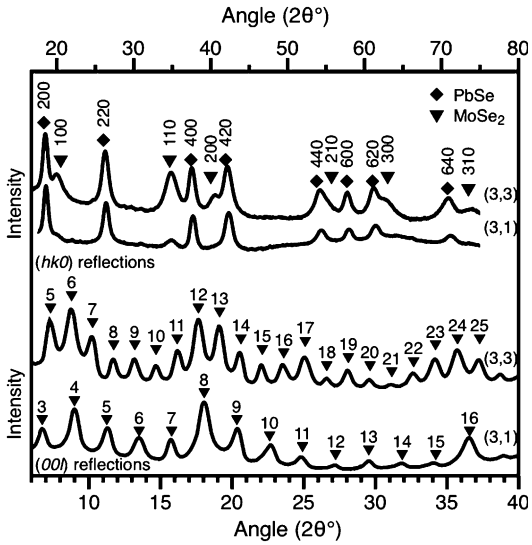

Figure 2. X-ray diffraction patterns acquired from structural variants $(m, n) = (3, 1)$, and $(3, 3)$ of $[(PbSe)_{1.00}]_m(MoSe_2)_n$. Bragg–Brentano patterns acquired using synchrotron radiation ($\lambda = 97.8$ pm) with the upper and lower pairs of patterns collected parallel and perpendicular to the plane of the films, respectively. Miller indices for the reflections are given above the patterns. For the bottom pattern, only the *l* value for the 00 L index is indicated.

The extended registry of the atomic planes along the modulation axis results in X-ray diffraction patterns (Figure 2) containing numerous $00l$ diffraction maxima, which can be used to determine the position of atomic planes along the *c* axis and hence independently quantify the structural distortions. The lattice parameters of the superstructure along the *c*-axis direction exhibit discrete changes of $\Delta c_m = 0.607 \pm 0.007$ nm and $\Delta c_n = 0.657 \pm 0.005$ nm as the number m or n of the PbSe or $MoSe_2$ structural units, respectively, is incremented. In-plane X-ray diffraction scans (Figure 2) contain Bragg diffraction maxima that can all be indexed based on independent crystal structures for the PbSe ($a = b = 0.617 \pm 0.005$ nm) and $MoSe_2$ ($a = 0.332 \pm 0.005$ nm) layers. The line widths of the reflections $hk0$ of the PbSe and $MoSe_2$ structural units differ, reflecting different in-plane domain sizes of 9 ± 1 nm for PbSe and 4 ± 1 nm for $MoSe_2$. There is no change in the lattice parameters or in-plane domain sizes as m and n increase and the films remain flat when removed from the substrate, suggesting that there is little residual strain despite the significant lattice mismatch between the layers. The random rotational variants observed in the PbSe between layers precludes the observation of coherent diffraction between layers along mixed-index hkl ($h,k \neq 0$; $l \neq 0$) directions. As shown in Figure 3 however, weak subsidiary maxima, denoted by white arrows, are observed along mixed-index reflections of the PbSe constituent. These maxima result from the finite size of the crystallites in these directions, as can be observed by the identical patterns observed for both (3, 1) and (3, 3) variants, which contain identical thicknesses of the PbSe constituent but have different *c*-axis lattice parameters. The diffraction data strongly suggest that the lattices of PbSe and $MoSe_2$ are not constrained by epitaxy at their interfaces, that the rock salt structured layers are crystallographically decoupled from one another, and that the layer thickness of one component does not affect the structure of the other.

Rietveld refinements of the $00l$ diffraction patterns were carried out on the first five compounds where $m = n$ in the related $[(PbSe)_{0.99}]_m(WSe_2)_n$ system. The structure with $(m, n) = (1, 1)$ is consistent with that previously reported for

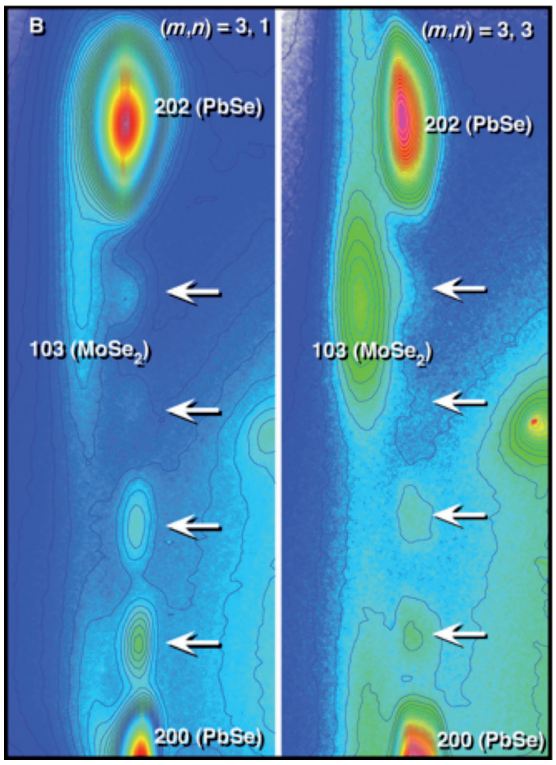

Figure 3. Two-dimensional in-plane patterns acquired using synchrotron radiation ($\lambda = 92.53$ pm). All peaks occur near reflections expected from the bulk crystal structures for PbSe and $MoSe_2$. The four weak reflections in each pattern, indicated with arrows, correspond to non-integer indices of PbSe of type 20*l*, as discussed in the text.

similar (1, 1) compounds.[20] The refinements reveal that the Pb and Se planes are separated by 21 pm, with the Pb in each of the distorted 001 planes of the rock salt structure displaced closer to the selenium of the dichalcogenide. This interfacial distortion or layer puckering is within the range (20 to 60 pm) previously reported. Refinements of other (m, n) family members in this system reveal that the PbSe planes are paired, as observed in the STEM-HAADF data of the $[(PbSe)_{0.99}]_m(MoSe_2)_n$ system in Figure 1, and that the puckering of the surface Pb-Se layer decreases as m, the number of structural units in the PbSe layer, increases. The difference between the intra-pair and inter-pair distances also decreases with increasing m and with greater distance from the PbSe–WSe_2 interface and is consistent with those shown in Figure 1.

To model the observed distortions, density functional theory (DFT) simulations were performed for isolated sheets of rock salt structured PbSe with layer thickness along the c axis ranging from one to five unit cells. Idealized PbSe structures of thickness $m \times c$ ($m = 1$ to 5; $c = 0.306$ nm) were allowed to relax to minimum-energy configurations. In the case of a single unit cell ($m = 1$), a strong reduction to $c =$ 0.283 nm is observed, while the a-axis lattice parameter remains unchanged. The experimentally observed pairing distortion for $m > 1$ is also observed; as m increases, the average c-axis lattice parameter approaches the bulk value. In the case of $m = 5$, the bulk PbSe structure is largely restored with only small distortions in the terminal units. These results provide additional evidence that the distortions are size dependent and decoupled from the dichalcogenide layers. Only a slight puckering (about 6 pm for $m < 5$; about 3 pm for $m = 5$) is observed for the surfaces of the relaxed PbSe layers. This distortion is significantly smaller than the experimentally observed value of 22 pm. The puckering, however, increases to 15 pm in the presence of the dichalcogenide layer in a model $[(PbSe)_{0.99}]_1(WSe_2)_1$ structure, likely resulting from Pb completing its coordination through bonding with the Se of WSe_2 and charge transfer between the WSe_2 and PbSe structural units.

Figure 4 contains a graph of the magnitude of the pairing distortion as a function of the number of PbSe structural units as calculated from the DFT simulations and as measured from the STEM images and the XRD pattern refinement. The

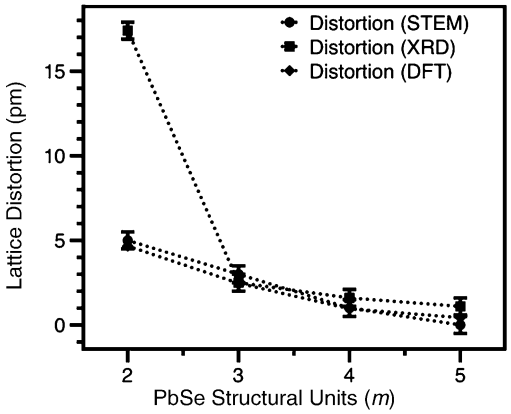

Figure 4. The change in the magnitude of the PbSe lattice distortion as layer thickness is increased. STEM and DFT data were collected using the $[(PbSe)_{1.00}]_m(MoSe_2)_n$ system while the XRD data was collected using $[(PbSe)_{0.99}]_m(WSe_2)_n$.

magnitude of the distortion decreases as the number of structural units, m, of PbSe increases. To our knowledge, this is the first experimental data that reveals the systematic change in nanostructure as a function of size. The value from Rietveld refinement and STEM values for the (2, 2) compound differ because the (2, 2) compound has a significantly larger layer puckering than the other compounds investigated. STEM-HAADF imaging has near Rutherford (about $Z^{1.7}$) atomic number dependence, with Pb providing a factor of three larger intensity than Mo and a factor of six larger intensity than Se, weighting the differences towards the position of higher Z containing planes. The STEM data is through a column of Pb and Se atoms and is weighted toward the Pb atom position whereas the X-ray distortion is calculated from the z coordinates resulting from the refinements.

Conceptually, the distortion of the rock salt structure arises from two distinct contributions: a distortion of the interface plane to optimize the interaction between the PbSe and $MoSe_2$ regions; and a volume distortion of the structure to minimize the total free-energy. The systematic structural distortions observed in PbSe as the number of structural units decreases has significant implications, perhaps explaining the

synthetic difficulties in isolating very small cluster sizes of extended structures. Our observations also suggest that structural distortions offer a possible root cause for the size dependency of physical properties at the nanoscale, and that discontinuities in physical properties with size should be expected for nanostructures as a consequence of these structural distortions.

Experimental Section

Samples were synthesized using modulated elemental precursors as described previously.[18] The crystalline quality, orientation, and thickness of the films were evaluated by high-resolution X-ray diffraction (XRD) and reflectivity (XRR). Cross-sectioned specimens for scanning (STEM) and conventional (TEM) transmission electron microscopy analysis were prepared using a variation of the small-angle cleavage method described by McCaffrey.[21]

Received: September 28, 2012
Revised: December 13, 2012
Published online: January 7, 2013

Keywords: chalcogenides · composites · hybrid materials · inorganic synthesis · nanomaterials

[1] C. N. R. Rao, G. U. Kulkarni, P. J. Thomas, P. P. Edwards, *Chem. Eur. J.* **2002**, *8*, 29.
[2] M. A. El-Sayed, *Acc. Chem. Res.* **2004**, *37*, 326.
[3] S. Sapra, J. Nanda, D. D. Sarma, *Encyclopedia of Nanoscience and Nanotechnology, Vol. 3* (Ed.: H. S. Nalwa), American Scientific Publishers, Stevenson Ranch CA **2004**, pp. 181 – 192.
[4] Y. G. Sun, Y. N. Xia, *Science* **2002**, *298*, 2176.
[5] Y. B. Mao, T. J. Park, S. S. Wong, *Chem. Commun.* **2005**, *46*, 5721.
[6] M. J. Yacamán, J. A. Ascencio, H. B. Liu, J. Gardea-Torresdey, *J. Vac. Sci. Technol. B* **2001**, *19*, 1091.
[7] W. W. Yu, Y. A. Wang, X. G. Peng, *Chem. Mater.* **2003**, *15*, 4300.
[8] V. F. Puntes, K. M. Krishnan, A. P. Alivisatos, *Science* **2001**, *291*, 2115.
[9] C. B. Murray, C. R. Kagan, M. G. Bawendi, *Science* **1995**, *270*, 1335.
[10] C. B. Murray, C. R. Kagan, M. G. Bawendi, *Annu. Rev. Mater. Sci.* **2000**, *30*, 545.
[11] E. V. Shevchenko, D. V. Talapin, N. A. Kotov, S. O'Brien, C. B. Murray, *Nature* **2006**, *439*, 55.
[12] S. H. Sun, C. B. Murray, D. Weller, L. Folks, A. Moser, *Science* **2000**, *287*, 1989.
[13] D. V. Talapin, E. V. Shevchenko, M. I. Bodnarchuk, X. C. Ye, J. Chen, C. B. Murray, *Nature* **2009**, *461*, 964.
[14] J. Chen, X. C. Ye, C. B. Murray, *ACS Nano* **2010**, *4*, 2374.
[15] L. O. Brown, J. E. Hutchison, *J. Phys. Chem. B* **2001**, *105*, 8911.
[16] S. J. L. Billinge, I. Levin, *Science* **2007**, *316*, 561.
[17] A. L. Rogach, D. V. Talapin, E. V. Shevchenko, A. Kornowski, M. Haase, H. Weller, *Adv. Funct. Mater.* **2002**, *12*, 653.
[18] Q. Y. Lin, M. Smeller, C. L. Heideman, P. Zschack, M. Koyano, M. D. Anderson, R. Kykyneshi, D. A. Keszler, I. M. Anderson, D. C. Johnson, *Chem. Mater.* **2010**, *22*, 1002.
[19] C. L. Heideman, N. Nyugen, J. Hanni, Q. Y. Lin, S. Duncombe, D. C. Johnson, P. Zschack, *J. Solid State Chem.* **2008**, *181*, 1701.
[20] G. A. Wiegers, *Prog. Solid State Chem.* **1996**, *24*, 1.
[21] J. P. McCaffrey, *Microsc. Res. Tech.* **1993**, *24*, 180.

